Multiple Equilibria, Periodic, and Aperiodic Solutions in a Wind-Driven, Double-Gyre, Shallow-Water Model

孙超 马佳良 刘群

Center for Earth System Science
Tsinghua University

Paper Authors: Shi Jiang, Fei-Fei Jin and Michael Ghil
Published in *Journal of Physical Oceanography*, 1994.

November 17, 2014

Outline

- Observation： the interannual variability of WBCs
- Theoretical studies： Veronis (1963), Charny and Flierl (1981)
- Wind-driven double-gyre system

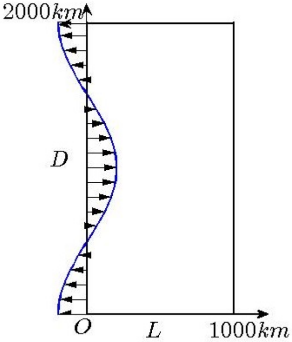

Figure 1: Wind stress $\tau^x = -\tau_0 cos(2\pi y/D)$.

- The reduced-gravity shallow water model

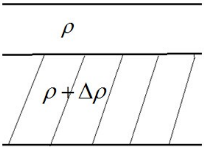

Figure 2: Reduced gravity shallow water model

Model Domain - Rectangular basin

$$0 \leqslant x \leqslant L, 0 \leqslant y \leqslant D$$

$$\frac{\partial U}{\partial t} + \nabla \cdot (\mathbf{v}U) = -g' h \frac{\partial h}{\partial x} + fV + \alpha_A A \nabla^2 U - RU + \alpha_\tau \frac{\tau^x}{\rho} \quad (1)$$

$$\frac{\partial V}{\partial t} + \nabla \cdot (\mathbf{v}V) = -g' h \frac{\partial h}{\partial y} - fU + \alpha_A A \nabla^2 V - RV \quad (2)$$

$$\frac{\partial h}{\partial t} = -\frac{\partial U}{\partial x} - \frac{\partial V}{\partial y} \quad (3)$$

$$\frac{\partial u}{\partial t} + u\frac{\partial u}{\partial x} + v\frac{\partial u}{\partial y} - fv = -g\frac{\partial h}{\partial x}$$

$$\frac{\partial v}{\partial t} + u\frac{\partial v}{\partial x} + v\frac{\partial v}{\partial y} + fu = -g\frac{\partial h}{\partial y}$$

$$\frac{\partial h}{\partial t} + \frac{\partial hu}{\partial x} + \frac{\partial hv}{\partial y} = 0$$

here

$$U\mathbf{i} + V\mathbf{j} = h\mathbf{v} = h(u\mathbf{i} + v\mathbf{j}) \quad (4)$$

is the upper layer mass flux vector.Coriolis parameter is given by $f = f_0 + \beta\gamma$, $g' = (\Delta\rho/\rho)g$ is reduced gravity.

Upper-ocean model

The upper layer of the ocean is driven by a zonal wind stress, τ^x.

$$\tau^x = -\tau_0 cos(2\pi y/D) \tag{5}$$

where τ_0 is the amplitude, τ^x is constant in time, but varies with latitude.
R: Rayleigh-type bottom friction scaled by *R* (Stommel, 1948)
A: Laplace-type lateral viscosity scaled by *A* (Munk, 1950).

Upper-ocean model - The boundary condition

The tangential boundary condition is a linear combination of tangential velocity and stress:

$$\gamma v + (1-\gamma) L_D \frac{\partial v}{\partial x} = 0 \quad \text{at} \quad x = 0, L \tag{6}$$

$$\gamma u + (1-\gamma) L_D \frac{\partial u}{\partial y} = 0 \quad \text{at} \quad y = 0, D \tag{7}$$

where $0 \leqslant \gamma \leqslant 1$, $\gamma = 0$ for the free-slip (no stress) and $\gamma = 1$ for the no-slip condition. L_D is the viscous-dissipation length.
(For simplicity, we use $\gamma = 1$ to analyse.)

Upper-ocean model

A convenient description of the globally oscillatory behavior of the system can be given in terms of total energy, and the total energy equation for the vertically integrated motion is

$$\frac{\partial(PE+KE)}{\partial t} = \mathscr{L} + \mathscr{R} + \mathscr{W} \tag{8}$$

Where

$$PE = \left\langle \frac{\rho}{2} g'(h-H)^2 \right\rangle, \text{Potential energy}$$

$$KE = \left\langle \frac{\rho}{2} h(u^2+v^2) \right\rangle, \text{Kinetic energy}$$

$$\mathscr{L} = \left\langle \rho A(u\nabla^2 U + v\nabla^2 V) \right\rangle, \text{Lateral friction}$$

$$\mathscr{R} = \left\langle -\rho R h(u^2+v^2) \right\rangle, \text{Bottom friction}$$

$$\mathscr{W} = \left\langle u\tau^x \right\rangle, \text{Wind stress}$$

(Note that the angle brackets denote a horizontal average over the entire basin)

Numerical results - a. Linear and nonlinear steady solutions

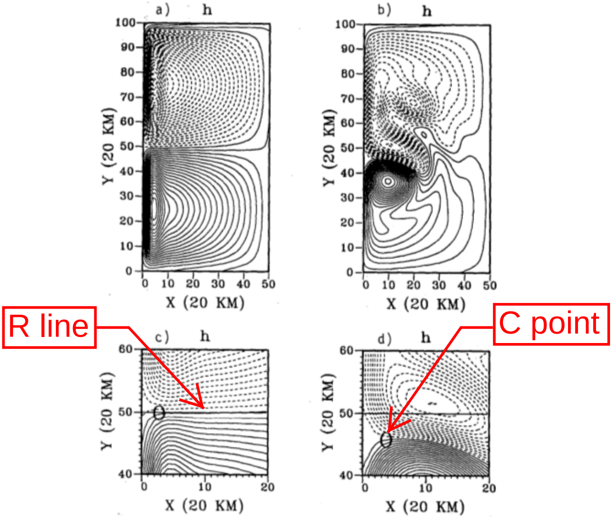

Figure 3: Steady-state upper-layer thickness h for (a) linear case and (b) nonlinear case; $\alpha_\tau = 0.95$, $\alpha_A = 1.3$; (c) and (d) are the enlarged insets corresponding to (a) and (b) with R line and the C point marked by a straight solid line and an oval, respectively. Solid curve stand for $h \geqslant 500$.

b. Multiple equilibria

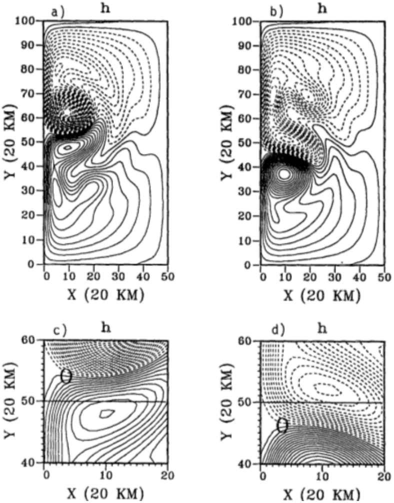

Figure 4: The h plot for multiple steady state in the nonlinear case; $\alpha_\tau = 0.9$, $\alpha_A = 1.3$. The initial state for (a) is a state of rest, while that for (b) is the same as Figure 3. Solid curves, dashed curves, and contour interval as in Figure 3.

c. Bifurcation diagram

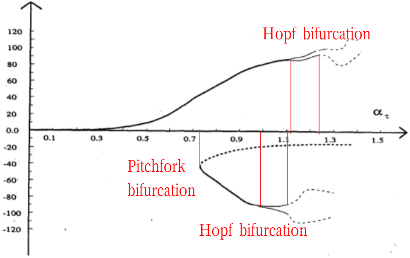

Figure 5: Bifurcation diagram for the position of C point, as a function of wind stress ($\alpha_A = 1.3$).

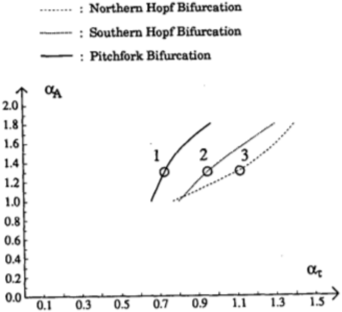

Figure 6: Catastrophe diagram in terms of the viscosity parameter α_A and the wind-forcing parameter α_τ

d. Periodic solutions

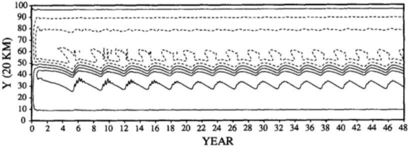

Figure 7: The periodic variations of h along $x = 80$ km for 48 years. The parameter values are $\alpha_\tau = 0.8$, and $\alpha_A = 1.0$. Solid and dashed lines as in Figure 3; contour interval is 20m.

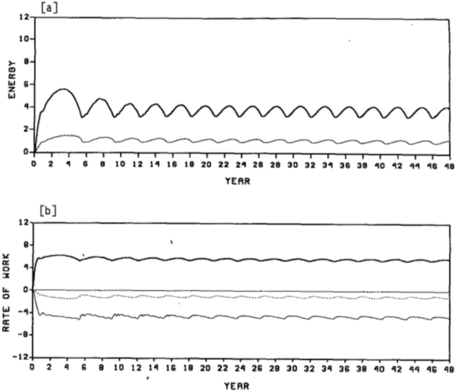

Figure 8: Time evolution of spatially averaged (a) energies $(10^{12} J \cdot m^2)$ and (b) energy rates $(10^{15} J \cdot m^2 s^{-1})$; $\alpha_\tau = 0.8$ and $\alpha_A = 1.0$. Panel a: thick line for available potential energy; thin line for kinetic energy; Panel b: thin line for frictional loss due to viscosity; dashed line for Rayleigh friction; thick line for wind forcing.

e. Aperiodic solutions

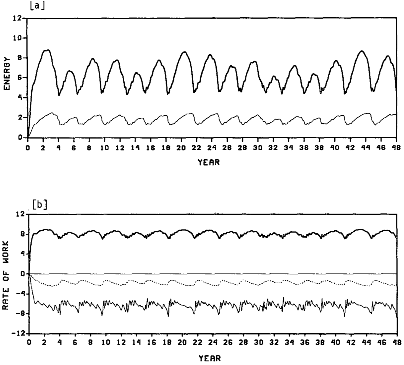

Figure 9: Time evolution of spatially averaged (a)(c) energies and (b)(d) energy rates;(a)(b):$\alpha_\tau = 0.95$ and $\alpha_A = 1.0$. Panel a: thick line for available potential energy; thin line for kinetic energy; Panel b: thin line for frictional loss due to viscosity; dashed line for Rayleigh friction; thick line for wind forcing.

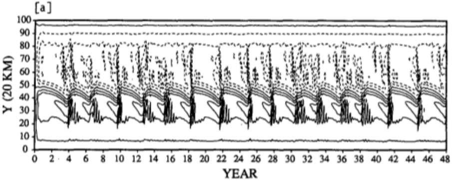

Figure 10: The variations of h along $x = 80$ km for 48 years. The parameter values are $\alpha_\tau = 0.95$ and $\alpha_A = 1.0$. Solid and dashed lines as in Figure 3; contour interval is 20m.

We reduced the original equations to low order ones with QG approximation:

$$\frac{\partial u}{\partial t} + \mathbf{v} \cdot \nabla u = -g' \frac{\partial h}{\partial x} + fv - Ru + \frac{\tau^x}{h\rho} \tag{9}$$

$$\frac{\partial v}{\partial t} + \mathbf{v} \cdot \nabla v = -g' \frac{\partial h}{\partial y} - fu - Rv \tag{10}$$

$$\frac{\partial h}{\partial t} = -\nabla \cdot (h\mathbf{v}) \tag{11}$$

Comparing to Eq.(1)-Eq.(4), we can know that we set $A = 0, \alpha_\tau = 1$.

a. Truncated QG model

The dimensionless QG equation corresponding to Eq.(9)-Eq.(11) is

$$\frac{\partial}{\partial t}(\nabla^2 - \lambda^2)\psi + R_0 J[\psi, (\nabla^2 - \lambda^2)\psi] + \frac{\partial \psi}{\partial x} = -\epsilon \nabla^2 \psi + w_f \tag{12}$$

$$w_f = -\frac{\partial}{\partial y}\left(\frac{\tau^x}{h}\right) \tag{13}$$

$\psi \Rightarrow$ streamfunction
$J \Rightarrow$ Jacobian

$L \Rightarrow$ horizontal scale
$H \Rightarrow$ vertical scales
$W \Rightarrow$ scale of the wind stress

$(t, x, y, h, \tau^x, \psi)$ in Eq.(12)-Eq.(13) are scaled by $(\beta^{-1}L^{-1}, L, L, H, W,$ $W\rho^{-1}\beta^{-1}H^{-1})$

a. Truncated QG model

The nondimensional parameter are defined as

$$R_0 = \frac{W}{\rho H \beta^2 L^3}, \epsilon = \frac{R}{\beta L}, \lambda = \frac{L}{L_R} \tag{14}$$

$L_R = \sqrt{g' H}/f_0 \Rightarrow$ internal Rossby radius of deformation

$R_0 \Rightarrow$ Rossby number, measure the effects of nonlinearity

$\epsilon \Rightarrow$ frictional parameter, measure the effects of fraction

$\lambda^2 \Rightarrow$ rotational Froude number

The boundary condition of no-normal flow requires that ψ varnish on all sidewalls, that is

$$\psi = 0 \begin{cases} \text{on} & x = 0, \pi \\ \text{on} & y = 0, \pi \end{cases} \tag{15}$$

a. Truncated QG model

We retain Veronis(1963) sine expansion in y direction, but a decaying exponential in x direction to account for the zonally asymetric structure. The limited set of basis functions used yields the expansions

$$\begin{gathered} \psi = A(t)F(x)\mathrm{sin}y + B(t)F(x)\mathrm{sin}2y \\ F(x) = e^{-ax}\mathrm{sin}x \end{gathered} \tag{16}$$

$$w_f = -w_1(x)\mathrm{sin}y - w_2(x)\mathrm{sin}2y \tag{17}$$

$$\begin{aligned}\frac{dA}{dt} - \mu AB + \nu A = \eta_1 \\ \frac{dB}{dt} - \mu A^2 + \nu B = \eta_2\end{aligned} \tag{18}$$

where

$$\mu = \frac{2aR_0}{\pi\lambda^2}\frac{1+e^{-a\pi}}{1+a^2}, \nu = \frac{2a}{\pi\lambda^2}$$

$$\eta_1 = \frac{\mathscr{F}_1}{\pi\lambda^2}, \eta_2 = \frac{\mathscr{F}_2}{\pi\lambda^2}$$

$$\mathscr{F}_1 = \int_0^\pi w_1 e^{ax} \sin x dx$$

$$\mathscr{F}_2 = \int_0^\pi w_2 e^{ax} \sin x dx$$

so that μ and ν are positive constants.

a. Truncated QG model

Eq.(18) can yields a steady states:

$$\begin{aligned} \mu AB - \nu A &= -\eta_1 \\ \mu A^2 + \nu B &= \eta_2 \end{aligned} \tag{19}$$

By eliminating B from Eq.(19), we can derive a cubic equation for A,

$$\mu^2 A^3 + (\nu^2 - \mu\eta_2)A - \nu\eta_1 = 0 \tag{20}$$

$\Rightarrow$ Pitchfork bifurcation equation

Analytic results - b. Bifurcation diagrams

$$\mu^2 A^3 + (\nu^2 - \mu\eta_2)A - \nu\eta_1 = 0$$

1) Purely symmetric wind stress curl

if $w_1 = 0$ and $\eta_1 = 0$, the steady state solutions are

$$\begin{cases} A_1 = 0 & \text{for all } \eta_2 \\ A_{2,3} = \pm\frac{\sqrt{\mu\eta_2 - \nu^2}}{\mu} & \text{for } \eta_2 \geqslant \frac{\nu^2}{\mu} \end{cases}$$

$\Rightarrow \eta_a = \frac{\nu^2}{\mu}$ bifurcation point

(see Figure 11 (a))

2) Nearly symmetric wind stress curl

If $w_1 \neq 0$ and $\eta_1 \neq 0$, the nature of the solutions of equation depends on the discriminant $\Delta \equiv (\frac{\nu\eta_1}{2\mu^2})^2 + (\frac{\nu^2 - \mu\eta_2}{3\mu^2})^3$

- $\Delta < 0 \Rightarrow \eta_2 > \eta_b = \eta_a + r\eta_a^{1/3}\eta_1^{2/3}$ $r = \frac{3}{\sqrt[3]{4}} \approx 1.9$. Three real solutions
- if $\eta_2 < \eta_b$, one root is real and two other roots are complex conjugate.

η_b is a saddle-node bifurcation point.

(see Figure 11 (b))

b. Bifurcation diagrams

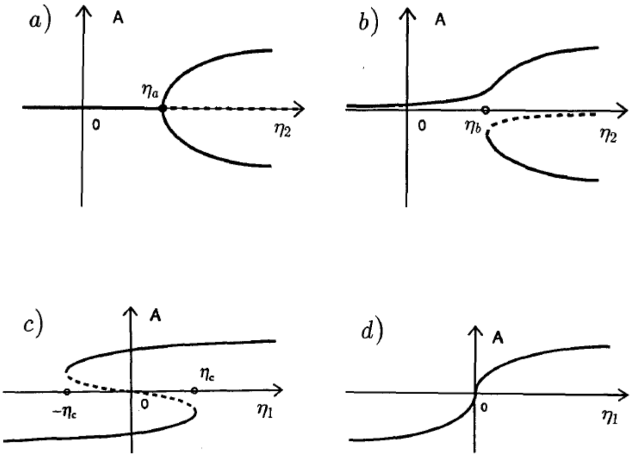

Figure 11: Analytic results for the simplified model: (a) pitchfork bifurcation with respect to η_2 when the wind stress is purely symmetric; (b) perturbed pitchfork bifurcation when the wind stress includes a small asymmetric component; (c) back-to-back saddle-node bifurcations with respect to η_1 at fixed $\eta_2 > 0$; and (d) the monotonic relation between the (unique) real steady solution and η_1 when the antisymmetric wind stress is dominant.

Discussion and conclusions

- Classical linear theory don't agree with many realistic nonlinear observations.
- Many theories try to explain these nonlinear behaviors to topography and other external forcings such as asymmetric wind.
- But the author think that the intrinsically nonlinear dynamics play a important role in determining the behaviors of WBCs.
- So this paper study the nonlinear behaviors of WBCs, including single equilibria, multiple equilibrias, periodic and aperiodic solutions.
- The exact physical causes for the separation and the contribution of intrinsic nonlinearity are still unclear.

The End

Thanks